30th NENE 2021
September 6 - 9
BLED-SLOVENIA
International Conference Nuclear Energy for New Europe

Effect of Heat Flux on Distribution of Vapour Volume Fraction and Bubble Size Distribution at Flow Boiling in Horizontal Annulus

Boštjan Zajec [1,2], Leon Cizelj [1], Boštjan Končar [1]
[1] Reactor Engineering Division
Jozef Stefan Institute
Jamova cesta 39
1000, Ljubljana, Slovenia
*bostjan.zajec@ijs.si, leon.cizelj@ijs.si, bostjan.koncar@ijs.si

[2] University of Ljubljana
Kongresni trg 12
1000, Ljubljana, Slovenia

ABSTRACT

Subcooled flow boiling was investigated in a horizontally placed annular test section. The installed experiment is a part of the laboratory THELMA (Thermal Hydraulics experimental Laboratory for Multiphase Applications) built at Reactor Engineering Division of Jožef Stefan Institute. The annular test section is constructed as a double-pipe heat exchanger, where the heat is transferred from the heating water flowing inside the inner copper pipe to the working fluid flowing through the annular gap between the inner pipe and outer transparent pipe that enables visualization of the boiling flow. Refrigerant R245fa is used as a working fluid as it boils at lower temperatures and lower pressures than water.

The main objective of this study is to investigate the effect of heat flux variation on the boiling flow patterns at approximately constant inlet flow conditions of the working fluid (fixed mass flux and inlet fluid temperature). The variation of heat flux was controlled by changing the mass flux of the heating water flow. Subcooled flow boiling of R245fa was recorded by a high-speed camera and images of the boiling flow were analysed using the image processing to determine the bubble size distributions. The experimental setup, analysis methods and measurement results are presented and discussed.

1 INTRODUCTION

Boiling flow is used as an efficient heat transfer mechanism in many systems, from air conditioners [1], power electronics cooling [2] and large power systems such as thermal power plants and nuclear reactors [3]. Despite its wide use, the prediction of heat transfer under specific conditions is difficult as it depends on many parameters. There is no single general mechanistic model with acceptable accuracy, thus predictions rely on many experimentally based correlations, suitable for specific fluids, geometries, flow orientations, surface types, pressures etc. Similarly, accurate numerical simulations of general two-phase flows are computationally too expensive. To reduce this cost, they still require some modelling by constitutional relations. Such simulations require validation by experimental data. Besides heat transfer and pressure drop prediction, bubble size, bubble departure frequency, vapour (i.e. void fraction) distribution are also important quantities to consider. With the advancement of high-

speed imaging techniques and analysis methods, the interest for detailed analysis of these quantities has increased. Although several authors have measured and described bubble size distributions in narrow channels, only a few papers describe these data in annular geometries.

Zeitoun et al. [4] investigated bubble behaviour in subcooled boiling of water in vertical annulus with inner tube diameter of 12.7 mm and 6.3 mm gap size. They used high-speed imaging and image processing to determine the mean bubble diameter after departure. Lee et al. [5] measured radial profiles of local void fractions in vertical annulus in subcooled boiling of water with 19.0 mm inner tube and 9.3 mm gap size. Two point-conductivity probes were used for local void fraction measurements. To the authors knowledge, the paper by Ugandhar et al. [6] is the only one describing the distribution of bubble sizes in a horizontal annulus. They have studied the effect of pressure on bubble size distribution in horizontal annulus (6.5 mm gap) with boiling water as a working fluid. High-speed camera was used and automated image processing was applied in Matlab. All mentioned experiments used electric resistance heating of the boiling surface.

In this paper, bubble distributions in horizontal annulus with 12.5 mm water-heated internal tube and 2 mm gap are measured. Refrigerant R245fa (pentafluoropropane) is used as a working fluid and a high-speed camera with manual image processing is used to determine the relative void fraction distribution per bubble size.

2 EXPERIMENTAL SETUP

The core of the experimental setup is a horizontal annular test section, thoroughly described in our previous works [7] [8]. Boiling occurs on the outer surface of the inner copper tube with a diameter of 12 mm and the total length of 585 mm. The annular gap between the copper tube and the outer glass tube is 2 mm wide. Outer surface of the copper tube is polished with sand paper grit 400 to provide a uniform distribution of nucleation sites. Boiling is observed with a high-speed camera through the borosilicate glass tube.

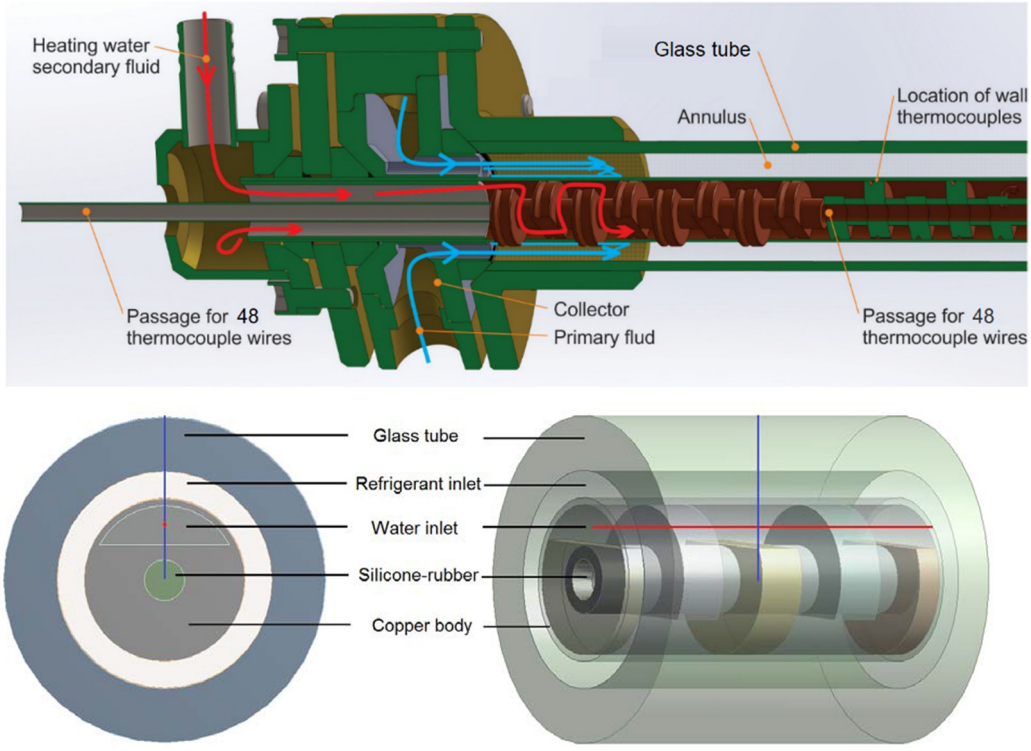

Figure 1: Schematic of the test section.

As the test section is designed as a concentric tube heat exchanger (see Figure 1), the supplied wall heat flux is temperature-controlled and there can be no overheating of the test section. Hot water flowing inside of a copper tube transfers the heat to the refrigerant flow (R245fa) in the annulus, which starts boiling on the copper tube outer surface at low temperatures (30°C at 1.8 bar). Finned structure inside of the copper tube provides strong heat transfer enhancement with homogeneous radial distribution and allows local temperature measurement along the tube axis. Thermocouples in contact with the heating water, positioned 21 mm apart, measure the local temperature of the water. For measurements in this study, refrigerant and water were flowing in the same direction to achieve maximum temperature difference between the water and refrigerant in the inlet region. Two thermocouples at the water and refrigerant inlets are used to measure the fluids inlet temperature. All thermocouples on the test section are referenced to the Kaye-170e artificial triple point of water and LabVIEW software was used for data acquisition. Two Micro Motion Emerson Coriolis flow meters are used for direct measurements of water and refrigerant mass flow rates. From these values, the mass flux (i.e. mass flow per unit of area) can be determined based on the cross-section area of the annulus.

For the visualization of the flow, a Phantom 12-bit grayscale high-speed camera is used with a 100 mm macro lens, enabling the observation area of approx. 3.6 x 1.6 cm on the test section. To reduce shadows and reflections on the recording, an even and diffuse lighting has been used. An U-shaped light was constructed from LED strips, illuminating the test section from all directions (except from the direction of the camera).

3 EXPERIMENTAL PROCEDURE

Experiments were performed in two series at constant refrigerant inlet conditions and at different temperatures of the heating water, to study the effect of the heat flux, separately from other possible effects. In our previous study [7], the influence of refrigerant mass flow rate was analysed at a constant inlet conditions of the heating water. In contrast to the current study, the changed refrigerant conditions, due to the test section design, inherently change also the heat flux [7].

For all cases considered in this study, the inlet water mass flow rate was kept constant at 25 kg/h (± 2%). Pressuriser was set at 30 ± 0.5 °C, which kept the inlet pressure stable in the range between 1.8 and 2 bar for all cases. Two sets of measurements were performed, one at refrigerant mass flux 150 kg/m^{2}s and the other at 300 kg/m^{2}s (± 1%), as presented in the Table 1. Water temperature was increased from 40 °C to approx. 70 °C between the cases. Due to malfunction of some thermocouples, heat flux was calculated from the inlet thermocouple to the first thermocouple on the test section, giving the average heat flux from inlet to the observed area.

Table 1: Experimental cases. Uncertainties stated in the first row apply to the whole column.

Name	Water inlet T [°C]	Refrigerant mass flux [kg/m^{2}s]	Heat flux [W]
150-40	40 ± 0.5	150 ± 3	50 ± 5
150-55	55	150	96
300-40	40	300	56
300-50	50	300	118
300-58	58	300	206
300-68	68	300	325

For each case, a steady-state of the system was first established. After that, the data was collected for 20 minutes and these time-averaged values are given in Table 1. Immediately after

the heat flux measurement, high-speed recording of boiling flow patterns was also performed. Recordings were done at 200 frames/s at the length of 10 second, yielding to 2000 flow images, which is sufficient to capture the flow patterns, as discussed in the next chapter. As the image of the test section without the bubbles was required for further post-processing, the boiling was temporarily terminated after each measurement. Heating water flow was turned off after each recording, stopping the boiling and an image of the test section with the single-phase flow background was recorded at exactly the same camera position, zoom and aperture settings.

4 IMAGE PROCESSING

For bubble detection, several different algorithms were tested, partly presented in our previous study [7]. Simple brightness detection or shape detection algorithms proved to be unsuccessful. Due to the annular geometry, bubbles in the free flow appeared darker than the background, while the bubbles in front of the copper pipe appeared lighter than the background. Larger bubbles also act as spherical lenses, containing basically the image of the whole test section in a single bubble. Such bubbles containing both bright and dark parts could not be properly detected with brightness patterns, no matter the shape-detection or edge-detection logic. As it was difficult to propose a mathematical description for such bubbles, neural network scheme was proposed.

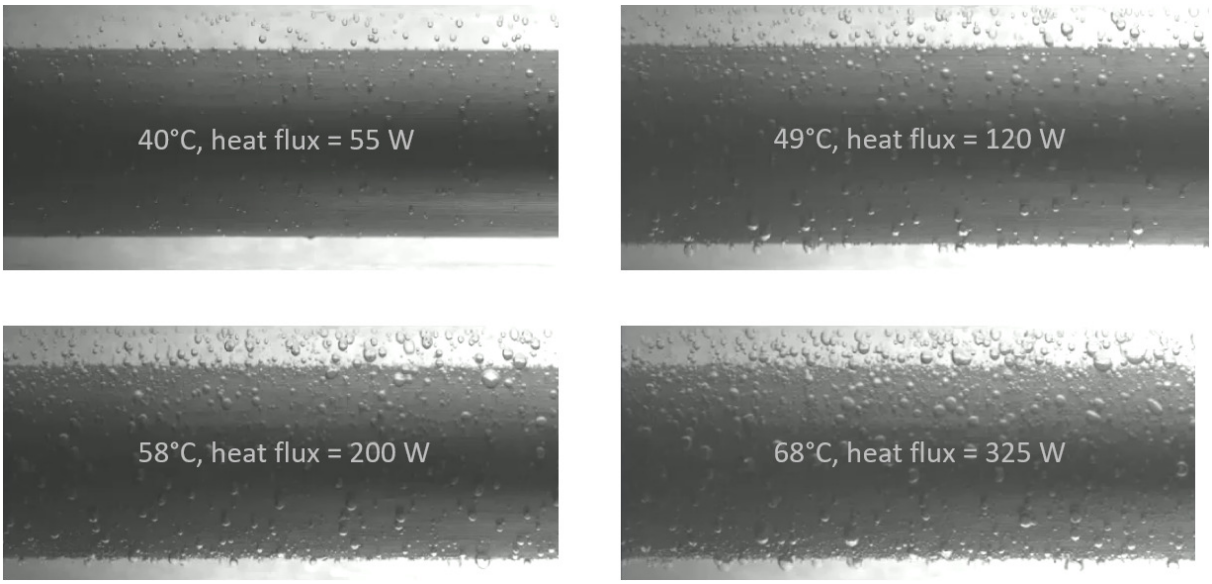

Figure 2: Boiling patterns at the same refrigerant inlet conditions and different heating water temperatures, corresponding to different surface heat fluxes.

In the first step, the empty background image was removed. Background subtraction was performed by dividing of each pixel value x_{img} (12-bit brightness) by the brightness of the pixel on the background image x_{bg}. Since brightness deviations could be present in both ways, the following equation for x_{final} was for used:

$$x_{final} = \sqrt{\left|1 - x_{img}/x_{bg}\right|} \tag{1}$$

Square root scaling was found to effectively highlight weak shades of bubbles, but other power function could also be used.

To detect bubbles with neural network, a relatively simple algorithm was proposed. First, a square window with size *a* is chosen, representing a bounding box of the bubble with dimeter

a. This window is then dragged across the flow image, starting at the top corner, and moving forward by one or two pixels in each iteration. After the end of the row, window is moved a step downward and again swept across the whole image width, until the whole image is scanned. In this way, a large number of largely overlapping windows are acquired. The task for the neural network is to determine whether the bubble is inside the window, whether it is centred and sufficiently large to fill the whole window. If these conditions are met, network output is "true" (valid window), while in every other case the output value should be "false" (invalid window). The algorithm is shown in Figure 3.

For training of the neural network, a similar window-dragging scheme was used. The bubbles were first manually marked on the image by providing a centre and diameter for each bubble. Differently sized windows were then dragged across the image and unless there was only one bubble inside the window and its diameter was not at least 90% of the window size, the window was fed in to the neural network as an invalid window. Such operation produced approximately one million of different inputs to the neural network from a single image with marked bubbles. Using the trial and error procedure, we have found out that training of the network based on the single flow image is the most appropriate. Training with multiple images drastically decreased recognition efficiency, by eliminating most of the bubbles. Such behaviour is likely a consequence of a too high learning parameter value used in the simple back-propagation learning scheme.

Based on experience of neural networks for hand-written number recognition from MNIST database [10] a fully-connected neural network with 625 input neurons, two hidden layers of 20 neurons and two output neurons for one-hot representation of true/false was chosen. Similarly, as with MNIST hand writing recognition, a whole bubble image (25 x 25 pixels = 625 inputs) is used as in input to the neural network. Both input and hidden layer sizes were chosen arbitrary and so far, no analysis of the other optimal configuration has been performed.

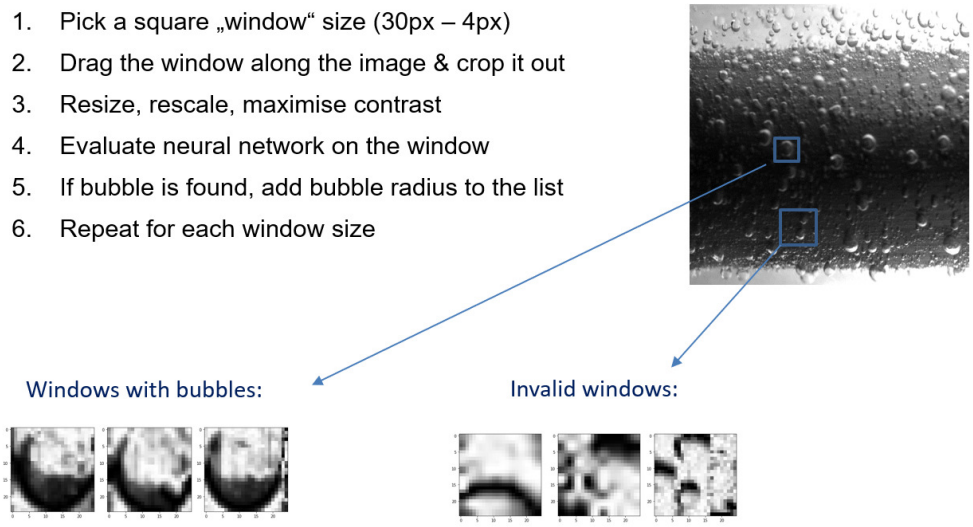

Figure 3: Bubble detection scheme

Due to its simplicity, the proposed bubble detection scheme is not very efficient, on a personal computer it is possible to process about 4 images per hour. As seen in Figure 4, the detection scheme is inefficient for larger bubbles and occasionally also gives false-positives, which requires additional manual inspection and processing of the results. However, the time needed for the manual detection of missing bubbles (marked in red in Figure 4) is much shorter than the manual detection of all bubbles, reducing the time of the whole process by about five times.

The convergence analysis has shown that if the images in the time frame between 0.2 s and 0.5 s are considered, approximately 5 to 10 images (depending on the case) already provide sufficient bubble statistics and bubble size distributions no longer change. Therefore, about 10 images from each set of 2000 images were used to calculate the bubble distribution. In future analysis, with faster (optimized) detection method, much larger number of images could be processed and since the same bubbles appear in multiple subsequent images, detection accuracy should also be improved.

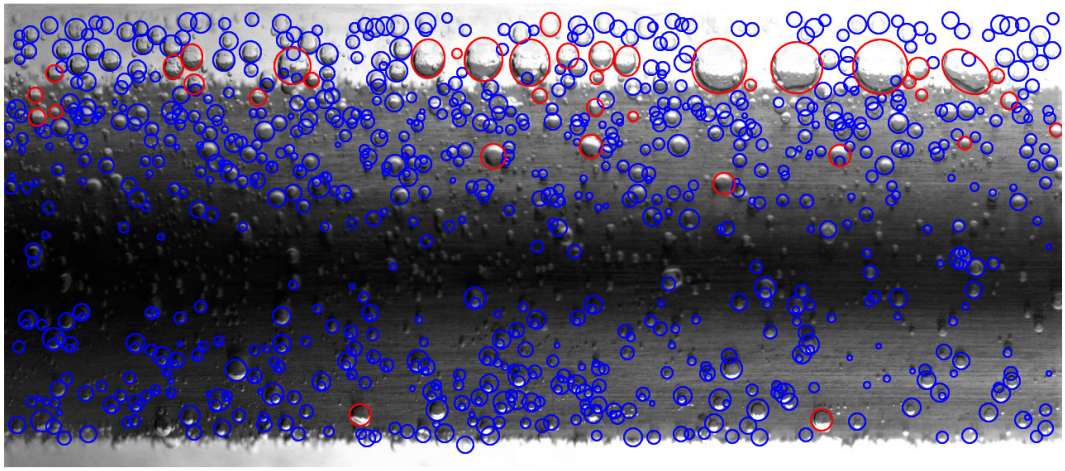

Figure 4: Image processed by neural network. Automatically detected bubbles are shown in blue while manually added bubbles are shown in red.

5 RESULTS AND DISCUSSION

Bubble size distributions resulting from image analysis are shown as histograms of the fraction of void volume. Such distribution shows the void volume contained in the certain bubble size normalized to the total void volume detected in the observed boiling flow pattern. So, the bubble sizes with meaningful contribution to the total void in the test section can be determined. The distributions shown in Figure 5 and Figure 6 show two distinct boiling flow behaviours.

For low refrigerant mass flux (150 kg/m^{2}s), presented in Figure 5, the distribution at low heat flux 50 W shows two separate peaks at bubble radii of around 0.15 mm and 0.5 mm, while the distribution at 96 W is more spread-out and there are no sharp peaks present.

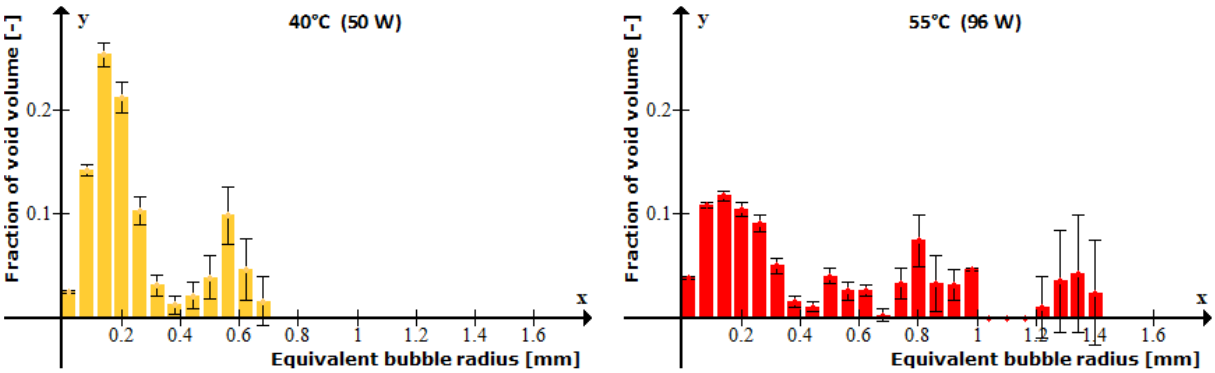

Figure 5: Bubble size distributions for low refrigerant mass flux (150 kg/m^{2}s).

Somewhat different flow behaviour is present at higher mass flux of 300 kg/m^{2}s, where single-peaked distributions are observed in all cases, regardless of the heat flux. For cases with

heat flux 118 W (300-49) and 206 W (300-58), the peaks could be approximated with a normal distribution. Distributions for higher heat flux cases at 206 W (300-58) and 325 W (300-68) are somewhat extended towards larger sized bubbles. It could be expected, that further increase of the heat flux would lead to the appearance of a more pronounced second peak. However, the current design of the experiment does not allow further increase of the heat flux, as the existing plastic pipes carrying the heating water cannot withstand water temperatures higher than 70°C.

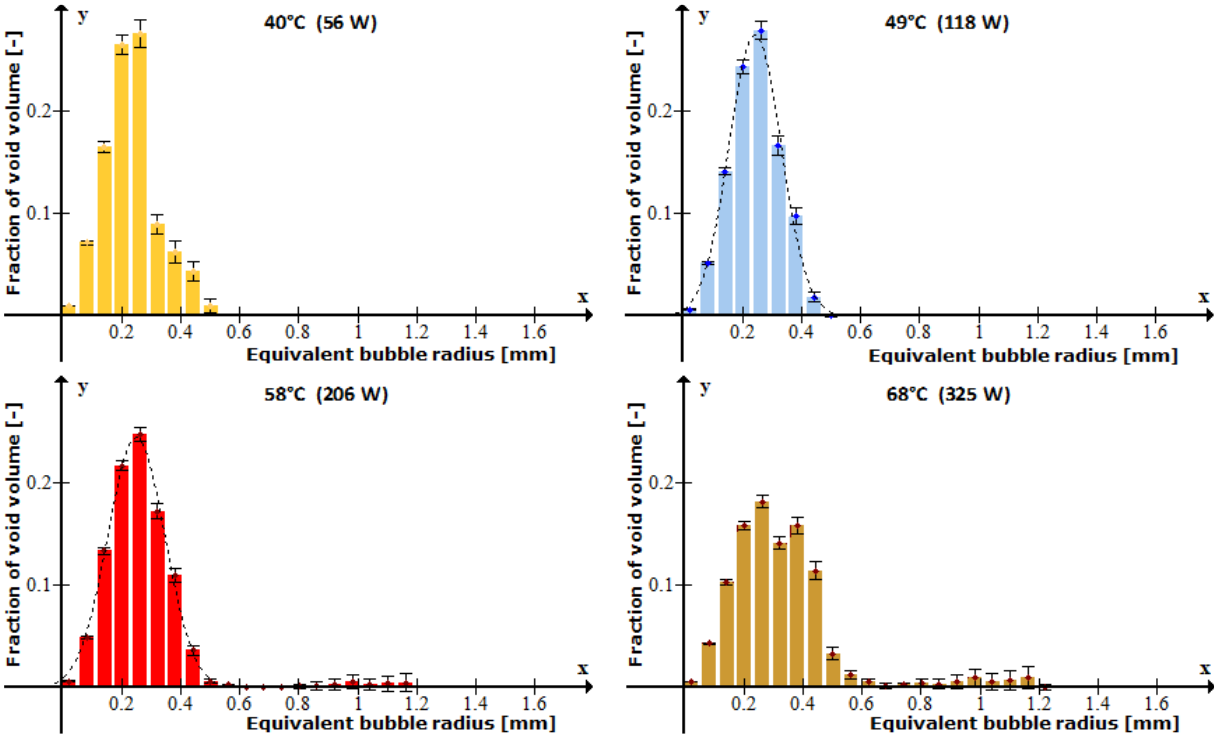

Figure 6: Bubble size distributions for higher refrigerant mass flux (300 kg/m^{2}s).

The observed non-gaussian distributions are a consequence of bubbles merging. At low mass fluxes, bubbles quickly rise to the top part of the test section where larger bubbles can be formed. At higher mass fluxes, larger bubbles are no longer observed for two main reasons. Firstly, merging of bubbles is less probable at higher mass flux to due to the higher fluid velocity, which carries the bubbles away from the surface. Secondly, due to the higher velocity, the bubbles formed at the bottom travel a longer path and leave the observation window before reaching the top. Downstream of the observation window, the bubbles may still merge at the top to form larger bubbles, but the local distributions change. Long tail of the distribution at the higher heat fluxes can be explained by the higher evaporation and larger number of bubbles at the surface. As a bubble moves through the liquid, it captures surrounding bubbles and is growing faster, both due to the ever-increasing cross-section and due to the increasing velocity. The observed tail in the distribution likely represents the bubbles at different stages of growth. Since the merging of bubbles depends on both, the liquid velocity and the amount of vapour, the distributions change with mass flux and heat flux, as presented in Figures 5 and 6.

6 CONCLUSIONS

A new set of measurements was performed at the existing test section, this time at constant refrigerant inlet conditions at different heat fluxes. The results at lower refrigerant mass flow rate have shown that the increased heat flux shifts the bubble size distributions from bimodal (two-peak) to more even and spread-out distribution. At higher refrigerant mass flow

rates, a different pattern is observed and single-peak distributions prevail. Only at the highest heat fluxes, some larger bubbles appear but with no pronounced peak in distributions.

Neural network was successfully applied for partly-automated bubble recognition, greatly speeding up the process of bubble distribution calculation. While the bubble recognition algorithm itself is fast enough for analysis of required number of images, more advanced neural network methods could further increase the speed and accuracy, completely eliminating the need for manual inspection of the results. Additional work on both checking the repeatability of experiments and accuracy of automated bubble counting is needed.

ACKNOWLEDGMENTS

The authors gratefully acknowledge dr. M. Matkovič for his contribution in design and building of the experimental apparatus for flow boiling studies in annular geometry. The authors also gratefully acknowledge the financial support provided by the Slovenian Research Agency through the grants P2-0026, L2-9210 and L2-1827.

REFERENCES

[1] S. Mancin, A. Diani and L. Rosetto, “Experimental Measurements of R134a Flow Boiling Inside a 3.4-mm ID Microfin Tube,” Heat Transfer Engineering, 2015, vol. 36

[2] L. Yeh, “Review of Heat Transfer Technologies in Electronic Equipment,” Journal of Electronic Packaging, vol. 117, 1995, pp. 333-339.

[3] B. Končar, E. Krepper and Y. Egorov, “CDF modeling of subcooled flow boiling for nuclear engineering applications,” in *Proceedings of the International Conference Nuclear Energy for New Europe 2005*, Bled, Slovenia, 2005.

[4] Zeitoun, O., and Shoukri, M. “Bubble Behavior and Mean Diameter in Subcooled Flow Boiling”. Journal of Heat Transfer, vol. 118, 1996

[5] T.H.Lee, G.C. Park and D.J. Lee, "Local flow characteristics of subcooled boiling flow of water in a vertical concentric annulus", International Journal of Multiphase Flow, vol. 28, 2020, pp. 1351-1368

[6] P. Ugandhar, A. Rajvanshi, A and D., Sarit. "Investigation of Bubble Behavior in Subcooled Flow Boiling of Water in a Horizontal Annulus Using High-Speed Flow Visualization", Journal of Heat Transfer. vol. 34, 2017, pp. 1-15.

[7] B. Zajec, B. Končar and L. Cizelj, “Heat Transfer Measurements and Visualization of Subcooled Flow Boiling of R245fa” NENE 2020, 29th International Conference Nuclear Energy for New Europe, Portorož, Slovenia, 2020

[8] M. Matkovič, L. Cizelj, I. Kljenak, B. Končar, B. Mikuž, A. Sušnik and I. Tiselj, “Building a Unique Test Section for Local Critical Heat Flux Studies in Light Water Reactor – Like Accident Conditions,” in Proceedings of the 13th International Conference on Heat Transfer, Fluid Mechanics and Thermodynamics (HEFAT), Portorož, Slovenia, 2017

[9] A. Kumar Basavaraj, B. Zajec and M. Matkovič, “Accurate measurements of the Local Heat Transfer coefficients along the dedicated test section,” in Proceedings of NENE 2018, 27th International Conference Nuclear Energy for New Europe, Portorož, Slovenia, 2018

[10] Y. LeCunn, C.Cortes, C. J.C. Cortes, “THE MNIST DATABASE of handwritten digits”, retrieved from http://yann.lecun.com/exdb/mnist/ on 25.10.2021